doi: 10.56761/EFRE2022. S6-O-012201

Investigation of negative glow plasma in helium and its application in gas analysis

A.I. Saifutdinov

Kazan National Research technical University named after A.N. Tupolev – KAI, Kazan, Russia
as.uav@bk.ru

Abstract. In this paper, within the framework of a self-consistent multilevel hybrid model, the kinetics of electrons in the negative glow region in similar glow discharges in helium at low and medium pressures is considered. The model is based on solving a two-dimensional kinetic equation for the electron distribution function written in the Fokker-Planck form and one-dimensional balance equations for the densities of charged and excited particles, the Poisson equation for an electric field. Within the framework of the model, the experimentally observed distributions of plasma parameters obtained using probe diagnostics are reproduced. The results are compared with the results of calculations obtained on the basis of an extended hydrodynamic model. Within the framework of the hybrid model, the formation of the spectrum of Penning electrons from impurities of complex molecules with an energy above the temperature of the main group of electrons is shown.
Keywords: negative glow, kinetic equation, hybrid model.

1. Introduction

The physics of non-equilibrium gas-discharge plasma is one of the rapidly developing areas of modern science. Such development is stimulated by wide applications of low-temperature plasma in various modern technical applications [1–4]. The most well-known non-equilibrium plasma generator is the classical DC glow discharge (GD) [5]. In addition to the cathode sheath, in which most of the potential drop is concentrated, there are two plasmas that are fundamentally different in nature: the plasma of the near-cathode region (the region of negative glow (NG) and Faraday dark space (FDS)), and the most studied plasma of the positive column [5]. In recent year more attention has been paid to near-cathode plasma. It is characterized by a low electron temperature (a few tenths of eV), a high density of charged particles [6–10], and a nonlocal EDF formation [7, 11].

It is near cathode plasma that has found new promising applications in the analysis of gas mixtures [9, 10, 12, 13]. In particular, the recent work [13] showed the possibility of identifying impurities of various complex inorganic and organic molecules. The technique is based on recording the spectra of fast electrons produced as a result of reactions of Penning ionization of impurity atoms or molecules. In this case, a necessary condition for the implementation of the method is the low temperature of the main group of electrons in the plasma and the non-locality of the EDF formation [12–14].

The aim of this work is to carry out numerical calculations of negative glow plasma in such glow discharges at low and high pressures in helium based on a multilevel self-consistent hybrid model. Particular attention is supposed to be paid to numerical confirmation of the possibility of detecting impurities of molecules using the example of methane in the near-cathode plasma of a glow discharge in helium.

2. Description of the model

The self-consistent hybrid model included two blocks: the first for describing the electronic component of the plasma and the second for describing the heavy component of the plasma (ions and excited particles).

To describe the spatial evolution of the electron distribution function (EDF) with respect to velocities, it is necessary to solve the Boltzmann kinetic equation [7]. The electron distribution function (EDF) depends on seven variables: spatial coordinates, velocity vector, and time. Since the operator of elastic collisions is the main one in the Boltzmann kinetic equation in a collisional plasma, its solution is expanded in terms of the eigen functions of this operator, i.e., spherical

functions [7, 15–18]. As a result, using the two-term approximation and passing in the kinetic equation from the coordinates "spatial coordinate-velocity" to "spatial coordinate and kinetic energy", we obtain [18]

$$\sqrt{w}\frac{\partial f_0}{\partial t}+\nabla_r\cdot\mathbf{\Phi}+\frac{\partial \mathrm{G}}{\partial w}=S_k\left(f_0\right), \tag{1}$$

in which the spatial and energy phase flows are written as follows

$$\mathbf{\Phi}=\frac{1}{3}\sqrt{\frac{2e}{m}}w\mathbf{f_1}=w^{1/2}D_r\left(\nabla-\mathbf{E}\frac{\partial}{\partial w}\right)f_0, \tag{2}$$

$$\mathrm{G}=\frac{1}{3}\sqrt{\frac{2e}{m}}w\mathbf{E}\cdot\mathbf{f_1}-\left[\left(\sum_k D_k\right)\frac{\partial}{\partial w}-\left(\sum_k V_k\right)\right]f_0. \tag{3}$$

Here, $S_k(f_0)$ is the inelastic collision integral, $D_r = v\lambda/3$ is the spatial diffusion coefficient. The coefficients D_k and V_k denote, respectively, the energy diffusion coefficients and the "friction forces" for collisional operators represented in the Fokker-Planck form: elastic and electron-electron collisions.

The coefficients for elastic collisions have the form

$$V_{elastic}=\chi\delta N_0\sigma_0(w)w^2,\ D_{elastic}=T_gV_{elastic}, \tag{4}$$

where N_0 is the gas density, $\sigma_0(w)$ is the elastic scattering cross section, and T_g is the gas temperature in electron volts.

For electron-electron collisions, the corresponding coefficients D_k and V_k were written in the form

$$D_C=\frac{4Y}{3\gamma^3}\left(\int_0^{w/\alpha}f_0(u)u^{3/2}du+w^{3/2}\int_{w/\alpha}^{\infty}f_0(u)du\right),\ V_C=\frac{2Y}{\gamma^3}\int_0^{w/\alpha}f_0(u)u^{1/2}du. \tag{5}$$

Here,

$$Y=\frac{Z^2e^4\ln\Lambda}{4\pi\varepsilon_0^2m^2},\quad \Lambda=\frac{12\pi\left(\varepsilon_0T_e\right)^{3/2}}{e^3n_e^{1/2}}, \tag{6}$$

$Z = 1$ is the charge of target particles (electrons) in units of e, ε_0 is the electrical constant, $\ln\Lambda$ is the Coulomb logarithm, n_e is the electron density, T_e is the electron temperature:

$$n_e=\int_0^{\infty}f_0(w)w^{1/2}dw,\quad T_e=\frac{2}{3n_e}\int_0^{\infty}f_0(w)w^{3/2}dw, \tag{7}$$

The inelastic collision integral is the sum of the different types of inelastic collisions. The corresponding terms for the processes of excitation, deexcitation, and ionization were written in the following form [7]:

$$S_k=-\gamma N_k\left(\sigma_k\left(w\right)wf_0(w)-a\sigma_k\left(\tilde{w}\right)\tilde{w}f_0(\tilde{w})\right),\ \tilde{w}=bw+\varepsilon_k, \tag{8}$$

where N_k, σ_k, ε_k are the density of heavy particles, the scattering cross section and the energy threshold for this process, respectively; $a = b = 1$ for excitation processes, $a = 4$, $b = 2$ for ionization processes. For superelastic collisions $\varepsilon_k < 0$ and $a = 0$, if $w < -\varepsilon_k$ (and $a = 1$ otherwise).

In addition, the collision integral includes Penning ionization. For it, the collision operator is an external source in the kinetic equation

$$S_p = R_p \theta(w), \tag{9}$$

Where R_p is the reaction rate of Penning ionization, $\theta(w)$ is a function describing the spectrum of electrons produced in this reaction and normalized to unity.

The boundary conditions for (3) in the configuration space were written as follows

$$\mathbf{\Phi} \cdot \mathbf{n}\big|_{x=0,L} = \frac{w}{2m} f_0 + (1-\alpha)\frac{m\gamma}{4\pi} g(w)(\mathbf{\Gamma}_i \cdot \mathbf{n}), \tag{10}$$

Here, the first term in the integration is the flux due to the chaotic motion of electrons, and the second term is the flux of electrons ejected from the cathode surface due to the process of secondary electron emission, described by the coefficient γ and determined by the ion flux to the cathode $\mathbf{\Gamma}_i$. The coefficient $\alpha = 1$ on the anode (at the point $x = L$) and $\alpha = 0$ on the cathode (at the point $x = 0$). The function $g(w)$ describes the spectrum of electrons emitted from the cathode, described using the Gaussian function. The boundary conditions for (3) in the energy space were written in the following form

$$G\big|_{w=0} = 0,\ G\big|_{w=w\max} = 0. \tag{11}$$

Let us proceed to the description of the second block of model equations. To describe elementary processes in a low-pressure helium discharge, one effective energy level and one type of ion were taken into account [19, 20]. To describe the discharge at medium and high pressure, three energy levels were taken into account: the triplet, singlet, and effective states of the helium atom, one excitation state of the helium molecule as well as two types of ions [21, 22] (The elementary kinetics will be described in more detail below). The spatial distributions of these particles were described using the continuity equations, and the self-consistent electric field was determined from the Poisson equation

$$\frac{\partial n_i}{\partial t} + \nabla \cdot \mathbf{\Gamma}_i = S_i - n_i / \tau, \tag{12}$$

$$\frac{\partial n_m}{\partial t} + \nabla \cdot \mathbf{\Gamma}_m = S_m, \tag{13}$$

$$\Delta\varphi = -\frac{e}{\varepsilon_0}(n_i + n_{i2} - n_e), \quad \mathbf{E} = -\nabla\varphi. \tag{14}$$

The ion fluxes were recorded in the diffusion-drift approximation

$$\mathbf{\Gamma}_i = -D_i \nabla n_i + \mu_i \mathbf{E} n_i, \tag{15}$$

$$\mathbf{\Gamma}_m = -D_m \nabla n_m, \tag{16}$$

where D_i, D_m are the diffusion coefficients of ions and excited atoms, and μ_i is the mobility of ions. The first terms on the right side of (15) and (16) describe the source and sink of ions S_i and metastable atoms, respectively. For ions, the source includes the processes of impact ionization, stepwise and Penning ionization, the sink of ions is described using the ambipolar diffusion of charged particles to the wall n_i/τ, where $\tau = (2.4R)^2/D_a$ is the effective time of ambipolar diffusion to the walls, D_a is the coefficient of ambipolar diffusion. For metastable particles, the source on the

right side of Eq. (16) includes excitation processes, while the sink is due to the processes of stepwise ionization, Penning ionization, and superelastic collisions.

To describe discharges at medium and high pressures, it is necessary to take into account gas heating, which leads to a redistribution of the density of neutral gas particles, on which the processes of excitation and ionization depend. In this connection, the energy balance equation for the heavy plasma component was additionally taken into account

$$\rho C_p \frac{\partial T}{\partial t} \nabla \cdot (\kappa \nabla T) = -e\mathbf{E} \cdot \mathbf{\Gamma}_i + S_{el}, \tag{17}$$

Where C_p is the heat capacity of helium at constant pressure, κ is the thermal conductivity of helium, the first term on the right-hand side describes the Joule heating by the ion current, and the second term describes the heating due to the transfer of energy from electrons to the heavy plasma component due to elastic collisions.

The boundary conditions for equations (15)–(20) were written as follows:

$$\mathbf{n} \cdot \mathbf{\Gamma}_i \big|_{x=0,L} = \left(\nu_{th,i} n_e / 4 \right) + \alpha \mu_i n_i \mathbf{E} \cdot \mathbf{n}, \tag{18}$$

$$\mathbf{n} \cdot \mathbf{\Gamma}_m \big|_{x=0,L} = \left(\nu_{th,m} n_m / 4 \right), \tag{19}$$

$$\varphi \big|_{x=0} = 0, \ \varphi \big|_{x=L} = U_0, \tag{20}$$

$$T \big|_{x=0} = T \big|_{x=L} = T_0, \tag{21}$$

Where $v_{th,i}$, $v_{th,m}$ are the average thermal velocities of ions and excited plasma particles, respectively, T_0 = 300K.

To describe elementary processes in a low-pressure helium discharge, we considered a simplified set of plasma-chemical reactions that takes into account the effective excited helium atom and positive ion (see Table 1).

Table 1. Simplified set of plasma-chemical reactions for elementary processes in a low-pressure helium discharge

№	Symbol	Energy (eV)	Statistical weight	Effective Level Components
1	He	0	1	1^1S_0
2	He^m	19.8196	3	2^3S_1
3	He^+	24.5874	1	He^+

In this case, the set of reactions presented in Table 2 was considered. In addition, a series of calculations were carried out with an extended set of plasma-chemical reactions to describe the discharge at medium pressures. Three kinds of excited helium atoms were considered: metastable triplet and singlet states, one effective excited level (with the principal quantum number n=3), two kinds of positive ions (see Table 3) and one kind of excited (metastable state) of molecular helium. A set of plasma-chemical reactions is presented in Table 4.

An additional excited atomic level was included in the model to take into account the process of associative ionization 12, in which molecular helium ions are formed. Singlet and triplet metastable atoms are converted into triplet atomic and molecular metastables, respectively, through the reactions 10 and 13. Singlet metastable atoms are also converted to ground state atoms by the 11 process. Atomic and molecular ions are formed in the processes of Penning ionization 14–20, leading to the loss of metastable excited particles and the formation of fast electrons. In addition, fast electrons are formed in superelastic collisions (de-excitation processes) 8–9. Atomic ions are

converted to molecular ions due to the 19 conversion process. The death of atomic and molecular ions are described using recombination processes 21–23.

Table 2. Reduced set of considered plasma-chemical processes in helium

№	Reaction	Reaction constant k_j, m^3/s	Description
1	$e + He \rightarrow e + He$	$f_0(\sigma,w)$ [19, 20]	Elastic scattering
2	$e + He \rightarrow e + He^m$		Excitation
3	$e + He \rightarrow 2e + He^+$		Direct ionization
4	$e + He^m \rightarrow 2e + He^+$		Stepwise ionization
5	$e + He^m \rightarrow He + e\{19.82eV\}$		Superelastic collisions
6	$He^m + He^m \rightarrow He^+ + He + e\{15.05\}$	2.4×10^{-15} [21, 22]	Penning ionization
7	$He^m + A \rightarrow A^+ + He + e\{E^m - E_{ion}\}$	2.4×10^{-15} [21, 22]	Penning ionization*

*A – Impurity molecules: CH_4, CH_3, C.

Table 3. Considered states of the helium atom at middle and high pressure

№	Symbol	Energy (eV)	Statistical weight	Effective Level Components
1	He	0	1	1^1S_0
2	He^T	19.8196	3	2^3S_1
3	He^S	20.6157	1	2^1S_0
4	He*	23.02	36	$3\,^3S_0$, $3\,^1S_1$, $3\,^3P_2^0$, $3\,^3P_1^0$, $3\,^3P_0^0$, $3\,^3D_3$, $3\,^3D_2$, $3\,^3D_1$, $3\,^1D_2$, $3\,^1P_1^0$, 3^3S_0, 3^1S_1, 2^3S_1
5	He^+	24.5874	1	He^+
6	He_2^+	24.5874	1	He_2^+
7	He_2*			He_2*

In determining the ionization and excitation constants of metastable helium atoms, data from the LxCAT project were used. In particular, for the reduced set of sections from Phelps [19], and for the extended set from L.Alves) et al. (IST-Lisbon) [20] and from [21, 22].

The reaction constants involving electrons were determined as follows

$$R_k = 8\pi N_k \left(\frac{w_0}{m}\right)^2 \int_0^\infty f_0(w)\sigma(w)\,w dw. \qquad (22)$$

3. Comparison of the results of numerical studies with experimental data. The discussion of the results.

The system of equations (1)–(3) and (12)–(17) with boundary conditions (10)–(11) and (18)–(21) was solved self-consistently by the finite element method. Three similar discharge tubes were considered with the similarity parameter pL = 0.6 kPa·cm at low, medium, and high pressures. Pure helium, as well as helium with small admixtures of methane (CH_4), was considered as the working gas.

On Fig.1a and Fig.1b show the distributions of the densities of electrons, ions, excited atoms and the distribution of the electron temperature, strength and potential of the electric field obtained in the framework of the hybrid model and the extended hydrodynamic model for a discharge at a pressure of p = 300 Pa and with an interelectrode distance L = 2 cm. The voltage drop was set to 250 V and the current density was j = 0.8 A/m^2.

The results obtained within the framework of the hybrid model demonstrate a low temperature of electrons in the negative glow plasma, which is 0.09–0.1 eV, while the electron density reaches m^{-3}. The results obtained within the framework of the extended fluid model give temperature values in the range from 2 to 4 eV and the maximum electron density m^{-3}, respectively. The distributions of the strength and potential of the electric field obtained in the framework of both models are similar.

Table 3. Extended set of considered plasma-chemical processes in helium

№	Reaction	Reaction constant k_j m^3/s or m^6/s	Description
1	$e^- + He \rightarrow e^- + He$	$f_0(\sigma,w)$	Elastic scattering
2	$e^- + He \rightarrow e^- + He^T$	$f_0(\sigma,w)$	Excitation
3	$e^- + He \rightarrow e^- + He^S$	$f_0(\sigma,w)$	Excitation
4	$e^- + He \rightarrow e^- + He^*$	$f_0(\sigma,w)$	Excitation
5	$e^- + He \rightarrow 2e^- + He^+$	$f_0(\sigma,w)$	Direct ionization
6	$e^- + He^T \rightarrow 2e^- + He^+$	$f_0(\sigma,w)$	Stepwise ionization
7	$e^- + He^S \rightarrow 2e^- + He^+$	$f_0(\sigma,w)$	Stepwise ionization
8	$e^- + He^T \rightarrow He + e^-\{19.82eV\}$	$f_0(\sigma,w)$	Superelastic collisions
9	$e^- + He^S \rightarrow He + e^-\{20.62eV\}$	$f_0(\sigma,w)$	Superelastic collisions
10	$He^S + e \rightarrow He^T + e\{0.79\}$	$f_0(\sigma,w)$	Mixing of excited levels
11	$He^S + He \rightarrow 2He$	8×10^{-21}	Quenching
12	$He^* + He \rightarrow He_2^+ + 2e^-$	8×10^{-17}	Associative ionization
13	$He^T + 2He \rightarrow He_2^* + He$	1.13×10^{-1} $mbar^{-2}s^{-1}$	Excimer formation
14	$He^T + He^T \rightarrow He^+ + He + e^-\{15.05\}$ $\rightarrow He_2^+ + e^-\{17.4\}$	1.5×10^{-15}	Penning ionization
15	$He^S + He^S \rightarrow He^+ + He + e^-\{16.65\}$ $\rightarrow He_2^+ + e^-\{19\}$	3.5×10^{-15}	Penning onization
16	$He^T + He^S \rightarrow He^+ + He + e^-\{15.84\}$ $\rightarrow He_2^+ + e^-\{18.2\}$	3×10^{-15}	Penning ionization
17	$He^T + He_2^* \rightarrow He^+ + 2He + e^-\{13.1\}$ $\rightarrow He_2^+ + He + e^-\{15.5\}$	2.5×10^{-15}	Penning ionization
18	$He^S + He_2^* \rightarrow He^+ + 2He + e^-\{13.9\}$ $\rightarrow He_2^+ + He + e^-\{16.3\}$	3×10^{-15}	Penning ionization
20	$He_2^* + He_2^* \rightarrow He^+ + 3He + e^-\{11.3\}$ $\rightarrow He_2^+ + He + e^-\{13.7\}$	1.5×10^{-15}	Penning ionization
19	$He^+ + 2He \rightarrow He_2^+ + He$	6.5×10^{-44}	Conversion
21	$He_2^+ + 2e^- \rightarrow He^* + He + e^-$	4×10^{-32}	Recombination
22	$He^+ + 2e^- \rightarrow He^{**} + e^-$	6×10^{-32}	Recombination
23	$He_2^+ + e^- + He \rightarrow He_2^* + He$	5×10^{-39}	Recombination

To validate the hybrid model, we carried out probe studies of the cathode plasma in helium in a tube with a radius of 1.7 cm and an interelectrode distance of 2 cm for various values of the

discharge current. A movable cylindrical probe with a radius of 0.7 mm and a length of 2 mm was placed between the electrodes. On Fig.2 shows the probe current-voltage characteristic, its first and second derivatives for a discharge of 1 mA. The second derivative (inset in Fig.2) shows a low-energy part corresponding to the main group of plasma electrons and a high-energy part corresponding to fast electrons.

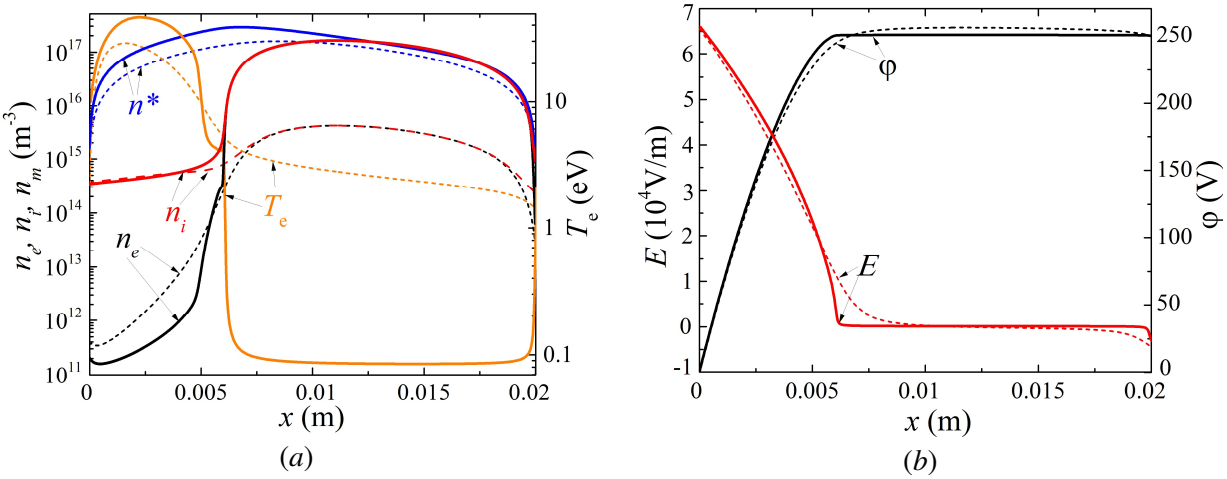

Fig.1. Distribution of *a*) the density of electrons, ions, metastable helium atoms and electron temperature and *b*) the strength and potential of the electric field along the discharge gap. The solid lines are for the results obtained within the framework of the hybrid model, the dashed lines are within the framework of the extended fluid model.

According to the slope of the logarithm of the second derivative of the probe CVC, in accordance with the probe theory [23], the temperature of the main group of electrons in the negative glow plasma was determined, which was T_e = 0.27 eV. From the ionic part of the probe CVC, the plasma electron density was determined, which was $n_e \sim n_i = 2.5\times10^{17}$ m^{-3}. As can be seen, the results presented in Fig.1a obtained within the framework of the hybrid model satisfactorily describe the experimental data.

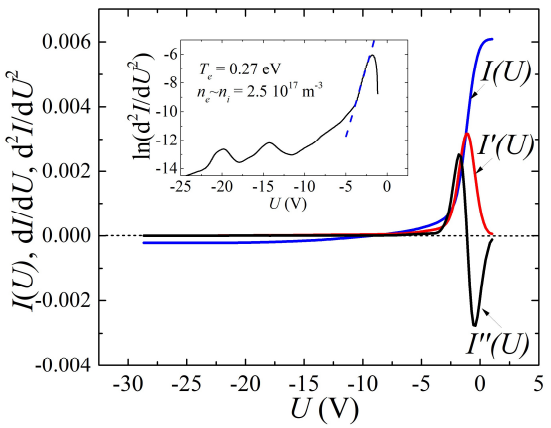

Fig.2. Probe characteristic, as well as its first and second derivatives in negative glow plasma. The inset shows the logarithm of the second derivative of the probe characteristic.

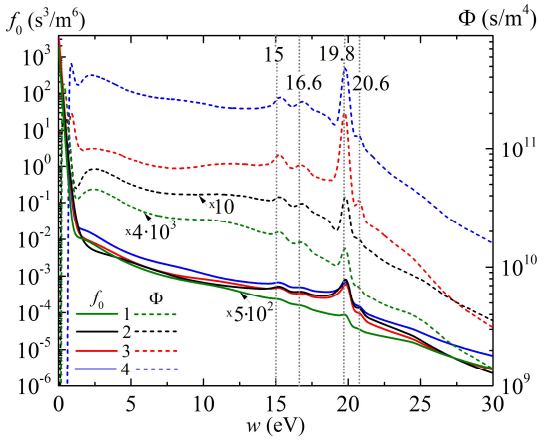

Fig.3. EDF (solid lines) and differential fluxes **Φ** (dashed lines) for conditions 1) L = 2 cm, p = 300 Pa, 2) L = 2 mm, p = 3 kPa; 3) L = 1 mm, p = 6 kPa; 4) L = 0.5mm, p = 12kPa.

Next, consider the EDF f_0 and differential fluxes **Φ** in the energy range 1 eV < w < 30 eV in the coordinate $x = 0.6L$ (Fig.4). On the fast part of the EDF, peaks are observed – the spectra of fast

electrons produced as a result of Penning ionization reactions and second-order impacts [9–14, 22]. It should be noted that characteristic peaks are observed more clearly on differential fluxes **Φ**, which is important from a practical point of view, since in practice, using a probe, the probe current is measured, which is proportional to f_1, and, consequently, to **Φ**.

Since the detection of fast electrons using probe methods has found application in gas analytical methods, it seems important to study the formation of narrow peaks in helium with low impurity contents. So, in Fig.4 shows the experimentally obtained high-energy part of the second derivative of the probe CVC in NG plasma in pure helium (corresponds to Fig.2), as well as in a He + 0.1%CH_4 mixture and in a He + 1%CH_4 mixture, at p = 30 Pa and L = 2 cm, obtained by double differentiation of the experimental probe CVC. Characteristic peaks are observed – the spectrum of fast electrons produced as a result of reactions of superelastic collisions and Penning ionization in pure helium and in a discharge with an admixture of methane:

$$\mathrm{He}(2^3S_1) + e \rightarrow \mathrm{He} + e\{19.82\mathrm{eV}\} \tag{23}$$

$$\mathrm{He}(2^1S_0) + e \rightarrow \mathrm{He} + e\{20.61\mathrm{eV}\} \tag{24}$$

$$\mathrm{He}(2^3S_1) + \mathrm{CH_4} \rightarrow \mathrm{He} + \mathrm{CH_4^+} + e\{6.9\mathrm{eV}\} \tag{25}$$

$$\mathrm{He}(2^3S_1) + \mathrm{CH_3} \rightarrow \mathrm{He} + \mathrm{CH_3^+} + e\{9.8\mathrm{eV}\} \tag{26}$$

$$\mathrm{He}(2^3S_1) + \mathrm{C} \rightarrow \mathrm{He} + \mathrm{C^+} + e\{8.6\mathrm{eV}\}, \tag{27}$$

$$\mathrm{He}(2^3S_1) + \mathrm{He}(2^3S_1) \rightarrow \mathrm{He^+} + \mathrm{He} + e\{14.5\mathrm{eV}\}. \tag{28}$$

A detailed analysis and possible channels of reactions that led to the formation of the resulting spectrum of fast electrons was carried out in [13].

Fig.5 shows the plasma at a point with coordinate x = 0.4L for different concentrations of methane impurities in helium. As can be seen from the results, characteristic peaks are observed from impurities produced as a result of Penning ionization reactions. Moreover, it can be seen that in the case of an impurity content of less than $1/10^5$ of the buffer gas, the peaks from impurities become unresolvable. Only peaks are observed from electrons produced in Penning ionization reactions involving two metastable helium atoms and electrons produced in superelastic processes.

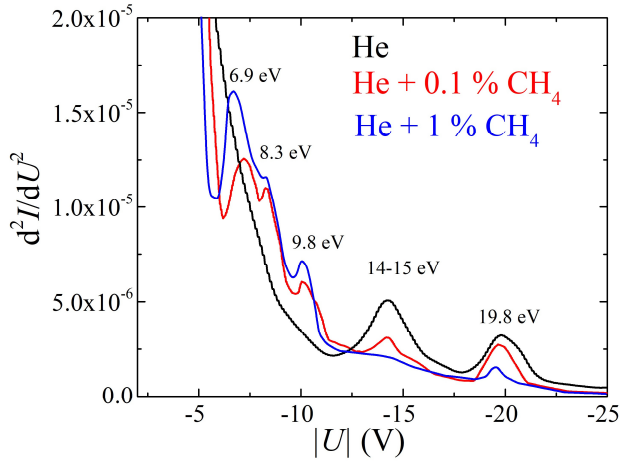

Fig.4. The second derivative of the high-energy part of the probe characteristic in pure helium, in a mixture of He + 0.1% CH4, and in a mixture of helium + 1% CH_4.

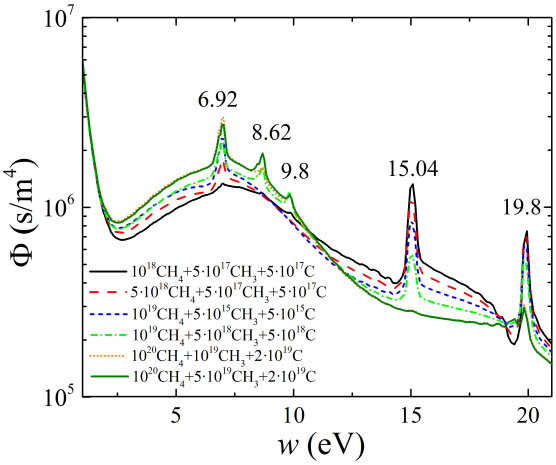

Fig.5. Differential flux **Φ** in the energy range 1eV < w < 21 eV in coordinate x = 0.4L obtained within the framework of the hybrid model for p = 300 Pa and L = 2 cm.

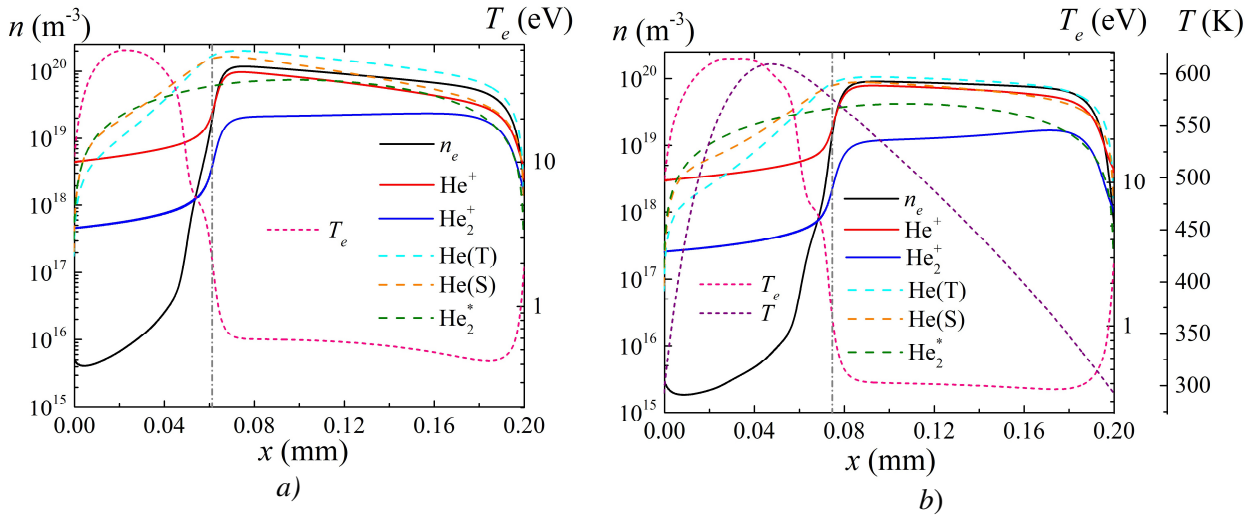

Fig.6. Distributions of the main plasma parameters for p = 30 kPa and L = 0.2 mm; *a*) without gas heating and *b*) with gas heating.

Similar studies were carried out at medium and high pressures, taking into account an extended set of plasma-chemical reactions. So in Fig.6 shows the main plasma parameters for p = 30 kPa and L = 0.2 mm with and without taking into account gas heating. It can be seen that taking into account the heating of the gas leads to a decrease in the electron temperature in the negative glow plasma and an increase in the cathode layer.

Fig.7 shows the EDF. It can be seen that the main group of electrons is not observed in the cathode sheath, but the fast part is visible. In the plasma region of the negative glow, both the slow part of the EDF and the fast part are observed

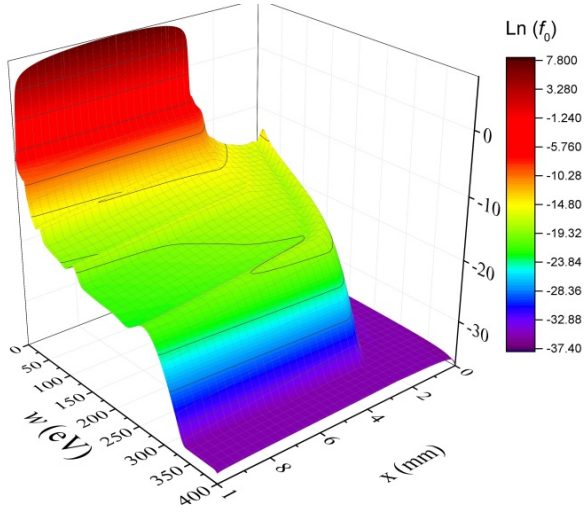

Fig.7. EDF in the discharge in three-dimensional form.

4. Conclusion

Thus, in the framework of the hybrid model, plasma was studied in the region of the negative glow of a glow discharge. The calculations showed the formation of a low temperature of the main group of electrons in the plasma, which corresponds to the experimental data obtained as a result of probe diagnostics. It is shown that the extended fluid model gives an overestimated temperature of several units of electron volts. Similar discharges are investigated at medium pressures. A slight deviation from the laws of similarity is shown. In addition, the energy dependences of the EDF and

differential flux showed the formation of narrow peaks from characteristic electrons produced as a result of the Penning ionization of impurities (methane and its derivatives) and metastable helium atoms. Numerical analysis showed the sensitivity of the method for determining impurities in negative glow plasma. It was one hundred thousandth, which corresponds to modern mass spectrometric methods.

Acknowledgement

The work was supported by a grant from the Foundation for the Development of Theoretical Physics and Mathematics "BASIS", project No. 21-1-3-53-1.

5. References

[1] Mariotti D., Sankaran R.M., *J. Phys. D: Appl. Phys*. **43**(32), 323001, 2010; doi: 10.1088/0022-3727/43/32/323001
[2] Wang X., Zhou M., Jin X., *Electrochimica Acta,* **83**, 501, 2012; doi: 10.1016/j.electacta.2012.06.131
[3] Arkhipenko V.I., et al., *Eur. Phys. J. D,* **66**, 252, 2012; doi: 10.1140/epjd/e2012-30359-x
[4] Korolev Y.D., *Russ J Gen Chem*, **85**, 1311, 2015; doi: 10.1134/S1070363215050473
[5] Raiser Yu.P., *Gas Discharge Physics.* (Moscow: Intellect, 2009).
[6] Derzsi A., Hartmann A., Korolov I., et al., *J. Phys. D: Appl. Phys*. **42**, 225204, 2009; doi: 10.1088/0022-3727/42/22/225204
[7] Kudryavtsev A.A., Smirnov A.S., Tsendin L.D., *Glow Discharge Physics (in Russian)*, (St. Petersburg: Lan', 2010).
[8] Bano G., et al., *PSST,* **16**, 492, 2007; doi: 10.1088/0963-0252/16/3/008
[9] Kudryavtsev A.A., et al., *Phys. Plasmas,* **24**, 054507, 2017; doi: 10.1063/1.4983620
[10] Saifutdinov A.I., Sysoev S.S., *PSST*, **30**(1), 017001, 2021; doi: 10.1088/1361-6595/abd61d
[11] Arslanbekov R.R., Kudryavtsev A.A., *Phys. Rev.* E **58,** 6539, 1998; doi: 10.1103/PhysRevE.58.6539
[12] Kudryavtsev A., Pramatarov P., Stefanova M., Khromov N., *Journal of Instrumentation*, **07**, P07002, 2012; doi: 10.1088/1748-0221/7/07/P07002
[13] Zhou Ch., et al., *PSST,* **30**, 117001, 2021; doi: 10.1088/1361-6595/ac3054
[14] Yuan Ch., et al., *Phys. Plasmas*, **25**, 104501, 2018; doi: 10.1063/1.5026214
[15] Tsendin L. D., *PSST*, **4**, 200, 1995; doi: 10.1088/0963-0252/4/2/004
[16] Zobnin A.V., Usachev A.D., Petrov O.F., Fortov V.E., *Phys. Plasmas,* **21**, 113503, 2014; doi: 10.1063/1.4901307
[17] Fedoseev A.V., Sukhinin G.I., *Plasma Phys. Rep.* **30,** 1061, 2004; doi: 10.1134/1.1839959
[18] Yan Ch., et al., *PSST*, **30**, 095006, 2021; doi: 10.1088/1361-6595/ac1df0
[19] Phelps database, private communication [online], retrieved on August 15, 2021; www.lxcat.net
[20] IST-Lisbon database, private communication [online], retrieved on August 15, 2021; www.lxcat.net
[21] Kutasi K., Hartmann P., Donko Z., *J. Phys. D: Appl. Phys.,* **34**, 3368, 2001; doi: 10.1088/0022-3727/34/23/308
[22] Martens T., Bogaerts A., Brok W., Dijk J.V., *Anal Bioanal Chem.*, **388,** 1583, 2007; doi: 10.1007/s00216-007-1269-0
[23] Saifutdinov A.I., Sysoev S.S., *Instrum Exp Tech* **65**, 75, 2022; doi: 10.1134/S0020441222010195